frontiers | Frontiers in Earth Science

TYPE Original Research
PUBLISHED 24 April 2023
DOI 10.3389/feart.2023.1093632

OPEN ACCESS

EDITED BY
Xander Wang,
University of Prince Edward Island, Canada

REVIEWED BY
Zhiyong Liu,
Sun Yat-sen University, China
Ahmed Kenawy,
Mansoura University, Egypt

*CORRESPONDENCE
Dengfeng Liu,
liudf@xaut.edu.cn
Tianling Qin,
qintl@iwhr.com

RECEIVED 14 November 2022
ACCEPTED 03 April 2023
PUBLISHED 24 April 2023

CITATION
Fan J, Wei S, Liu D, Qin T, Xu F, Wu C, Liu G and Cheng Y (2023), Impact of ENSO events on meteorological drought in the Weihe River basin, China.
Front. Earth Sci. 11:1093632.
doi: 10.3389/feart.2023.1093632

Impact of ENSO events on meteorological drought in the Weihe River basin, China

Jingjing Fan[1,2], Shibo Wei[1,2], Dengfeng Liu[3]*, Tianling Qin[4]*, Fanfan Xu[1,2], Chenyu Wu[1,2], Guanpeng Liu[1,2] and Yao Cheng[1,2]

[1]College of Water Resources and Hydropower, Hebei University of Engineering, Handan, China, [2]Hebei Key Laboratory of Intelligent Water Conservancy, Hebei University of Engineering, Handan, China, [3]State Key Laboratory of Eco-hydraulics in Northwest Arid Region, School of Water Resources and Hydropower, Xi'an University of Technology, Xi'an, China, [4]China Institute of Water Resources and Hydropower Research, Beijing, China

El Niño–Southern Oscillation (ENSO) events influence elements of the terrestrial water cycle such as precipitation and temperature, which in turn have a significant impact on drought. This work assessed the impact of El Niño and La Niña on droughts from 1970 to 2020 in the Weihe River basin (WRB) in China. This study used a standardized precipitation index (SPI) to characterize meteorological drought. The regional drought response to extreme events in El Niño/La Niña was analyzed using principal component analysis (PCA), Wilcoxon and Mann–Whitney tests, and other methods. The results showed that, based on PCA, the WRB is divided into two regions, with the northwest region (67%) comprising more area than the southeast region (33%). El Niño/La Niña significantly impacted drought in the WRB. Droughts mainly occurred in the El Niño year and the year following La Niña. El Niño had the highest number of drought years (44%), followed by the year following La Niña (43%). The number of droughts was lowest in the year following El Niño (22%). At 1-, 3-, and 6-month timescales, significant droughts mainly occurred from July to December in El Niño years and the summer following La Niña. On a 12-month timescale, significant droughts mainly occurred from January to April in El Niño years, while no droughts occurred in La Niña years. The longer the timescale of the SPI, the more months of significant drought in El Niño years; however, the intensity of drought in the basin was reduced. In the year following La Niña, summer droughts intensified on a 6-month timescale compared to a 3-month timescale. El Niño and La Niña had greater impacts on the drought index in the northwest region of the WRB. In the northwest region, 60% of the months showed significant drought, compared to only 2% of the months in the southeast region. The drought intensity was higher in the northwest region. The results of this study provide a reference for drought management and early warning systems in the WRB and support solutions to water shortage.

KEYWORDS

El Niño, La Niña, drought analysis, standardized precipitation index, arid and semi-arid region

1 Introduction

In the context of global warming, droughts are likely to become more severe and frequent (Dai, 2013; Singh et al., 2022). Drought is a recurrent natural phenomenon caused by chronic water deficits compared to normal conditions (Jim´enez-donaire et al., 2019; Sen et al., 2020). Although droughts have devastating effects on agriculture, ecology, and society, they are the least understood

and costliest natural disasters worldwide (Markonis et al., 2021; Xu et al., 2021; Peng et al., 2020). Since the 1970s, frequent drought events have seriously impacted the quality of life of people, as well as industry, agriculture, and national economic development (Ma and Ren, 2007; Trenberth et al., 2014; Zhang Q. et al., 2018). China is located in the East Asian monsoon region, which is densely populated, economically developed, and a sensitive and high-risk area for climate change. Approximately 20 million hectares/year of farmland is affected by drought, accounting for 60% of the area affected by all types of meteorological disasters, resulting in a reduction in food production from millions of tons to over 30 million tons (Zhang et al., 2008; Zhou et al., 2018). However, drought is a serious threat to food security and ecological safety, as well as to human survival and development (Su et al., 2018; Dai et al., 2022).

The El Niño–Southern Oscillation (ENSO) is the strongest interannual variability in the global climate system produced by sea–air interactions (Bjerknes, 1969). ENSO warm (El Niño) and cold (La Niña) phase events occur approximately every 2–7 years, usually starting to develop during the Northern Hemisphere summer and peaking at the end of the year or early in the following year (Yan, 2022). El Niño refers to the warmer surface water temperature in the equatorial eastern Pacific, while La Niña is the colder surface water temperature in the eastern equatorial Pacific (Luo, 2020). ENSO-driven precipitation anomalies have important implications for SST anomalies, surface wind fields, and oceanic thermocline changes (Kug et al., 2009; Okumura, 2019). Meanwhile, ENSO-driven tropical precipitation anomalies significantly affect global climate (Kim and Kug, 2018; Yeh et al., 2018). In the context of global warming, the average global surface temperature is approximately 1.0°C warmer than in the past, seriously affecting the global climate system (IPCC, 2018; IPCC, 2021; IPCC, 2022). The ENSO-driven positive precipitation anomalies in the equatorial Pacific both show a significant strengthening and eastward shift, leading to an eastward shift of the main variability modes of the Walker circulation and the ENSO-driven atmospheric teleconnections in the North Pacific and North America (Zhou et al., 2014; Kug et al., 2010; Bayr et al., 2014; Perry et al., 2017).

ENSO significantly affects human social activities through its tropical precipitation anomalies, which impact agriculture, the economy, ecosystems, and extreme events. These phenomena include wildfires in Southern California due to La Niña in 2017 and drought in SA due to El Niño in 2018–2019 (Yeh et al., 2018). The La Niña event is a key influence on the occurrence of prolonged droughts in northern China during spring and summer (Zhang L. et al., 2018). The persistent drought in northern China in 2010 is also closely related to the La Niña event (Shen et al., 2012). The La Niña event is one of the main drivers of the frequent cold weather in the eastern part of the country during the first winter of 2021 (Zheng et al., 2021; Zheng et al., 2022). The El Niño event was an important reason for the intensification of autumn drought in southern China after 1990 (Zhang et al., 2014). The severe meteorological drought in southern China in the autumn of 2019 is inextricably linked to the El Niño event (Ma et al., 2020).

Many studies have evaluated ENSO's impact on the climate. However, as the complex diversity of ENSO increases, the climate impact of tropical sea–air variability becomes unstable and its impact on drought in China becomes increasingly complex. The Weihe River basin (WRB) is located in the Loess Plateau, which has one of the largest rates of soil erosion on Earth (Zhou et al., 2022). The annual sediment discharge in the Loess Plateau is about 1.28 billion tons (Zhang et al., 2010). In addition, the WRB is an arid and semi-arid region, with precipitation primarily in summer, resulting in an uneven spatiotemporal distribution of water resources (Feng et al., 2022). More recently, the streamflow of the WRB has decreased significantly to 60% below the climate change (Guo et al., 2014). This decrease has led to increased shortages of water resources, which restrict the water ecological environment protection and economic and social development of the WRB (Yue et al., 2021). No studies have reported on the impact of El Niño/La Niña on drought in the WRB based on the classification of meteorological stations. Therefore, this study applied classification methods (e.g., principal component analysis) to cluster meteorological stations to better study the impacts of El Niño/La Niña on drought in the WRB.

The objective of this study was to reveal the impact of El Niño/La Niña on meteorological droughts in the WRB, an arid and semi-arid area in the northwest of China. This study classified 16 meteorological observation stations based on principal component analysis (PCA) to determine the partition. The characteristics of drought variation in El Niño/La Niña years and the following years were then analyzed and the influence of El Niño and La Niña on meteorological drought was investigated. The results revealed the mechanism of the influence of ENSO events on meteorological droughts to enhance understanding of the formation of meteorological droughts, which has important implications for the climate prediction of future meteorological droughts.

2 Study area

The WRB (104°00′E–110°20′E, 33°50′N–37°18′N) is the largest tributary of the Yellow River and covers a drainage area of 1.35×10^5 km^2. The river originates from Gansu Province and flows into the Yellow River at Tongguan Port, with a length of approximately 818 km (Hu et al., 2022) (Figure 1). The elevation of the WRB gradually decreases from west to east from 3926 to 325 m. The annual precipitation and air temperature of the WRB range from 500 to 800 mm and 7.8–13.5°C, respectively (Chang et al., 2015; Zhang T. et al., 2022). The precipitation within the basin is spatially uneven and exhibits a declining trend from southeast to northwest. The WRB is the main grain-yielding area and an important industry and commerce area in Northwestern China. The establishment of the Guanzhong–Tianshui economic zone will greatly promote the economic development of the whole western region (Chang et al., 2015). The geographical location is unique. The upstream area is located in the hilly area, while the middle reaches span the Loess Plateau. Soil erosion is serious, and the ecological environment is fragile (Li C. et al., 2019). Frequent droughts in the basin have increasingly serious economic, social, and ecological impacts (Ma et al., 2022).

3 Data and methodology

3.1 Data

This study used monthly precipitation and temperature data from 16 meteorological observing stations in the WRB from 1970 to 2020.

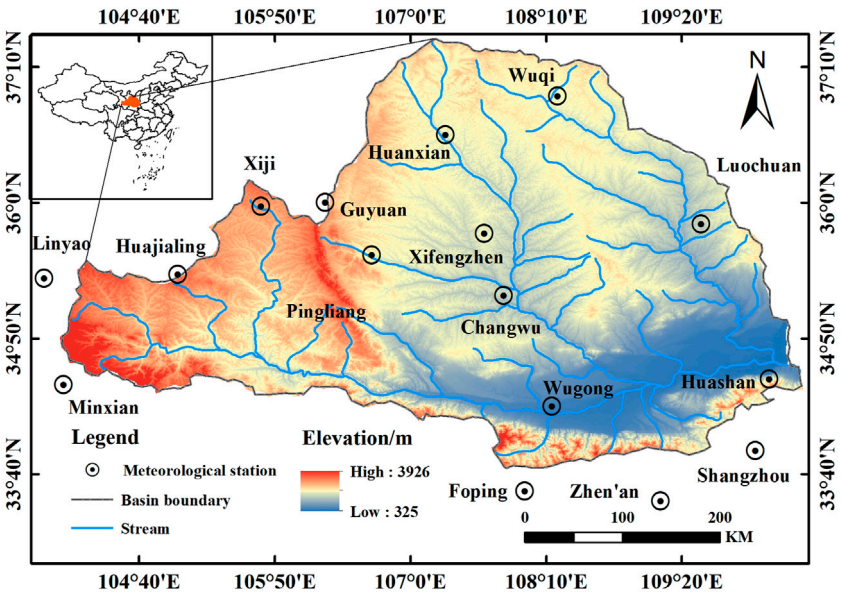

FIGURE 1
Geographical location of the Weihe River basin and distribution of each meteorological station.

These observed meteorological data were downloaded from the National Meteorological Information Center of China (https://data.cma.cn/). The monthly precipitation data were used to calculate the standardized precipitation index (SPI). According to the El Niño/La Niña Event Discriminatory Method developed by the Chinese Meteorological Administration, an El Niño (La Niña) event was defined as a 3-month sliding NINO3.4 index average of ≥0.5°C (≤−0.5°C) lasting for at least 5 months (Zhang et al., 2021). El Niño and La Niña historical events were obtained from the National Climate Center of China Meteorological Administration (http://cmdp.ncccma.net/download/ENSO/Monitor/ENSO_history_events.pdf). Nine peak years of El Niño events of moderate intensity or higher (1972, 1983, 1987, 1992, 1994, 1997, 2002, 2009, and 2015) and eight peak years of La Niña events of moderate intensity or higher (1971, 1973, 1975,1988, 2000, 2008, 2010, and 2020) and the following year since 1970 were selected for analysis (El Niño/La Niña years) to explore the impact of El Niño/La Niña on drought in the WRB.

3.2 Principal component analysis

Differences in the spatial distribution of precipitation in the WRB are influenced by the location of the sea and land, the western Pacific subtropical high-pressure system, and the Mongolian high-pressure system (He et al., 2012). The complexity of the monthly precipitation series in the WRB showed significant spatial differences, with the eastern part higher than the western part and the southern part higher than the northern part (Yang et al.; Liu et al., 2022). Therefore, before analyzing the impact of El Niño and La Niña on drought, the 16 meteorological stations were divided into two typical principal component site categories through PCA of the monthly precipitation series. PCA was first developed by Karl Pearson in 1901 (Vicente-Serrano, 2005; Badakhshan et al., 2021).

PCA is a multivariate statistical method used to reduce statistical indicators (Rutledge, 2018; Gao et al., 2020). Generally, the comprehensive indicators generated by the transformation are called principal components, and each principal component is a linear combination of the original variables (Arslan, 2009). The number of components was selected according to the criteria of an eigenvalue >1, and the components were rotated (varimax) to redistribute the final explained variance and to obtain more physically stable and robust patterns (Richman, 1986). The spatial classification of monthly precipitation patterns in the WRB was performed using the factorial loading values of each component obtained to group the observatories by the maximum loading rule. Each observatory was assigned to the component with the highest loading value.

3.3 Standardized precipitation index

The standardized precipitation index (SPI) was used as a meteorological drought index. The value was determined by normalizing the long-term precipitation record for the desired period for a given station after it was fitted to a probability density function, as described by McKee (Prajapati et al., 2021). The SPI only considers the deficit of precipitation. This study divided drought into four categories according to the SPI value: mild ($-1 < SPI \leq -0.5$), moderate ($-1.5 < SPI \leq -1$), severe ($-2 < SPI \leq -1.5$), and extreme ($SPI \leq -2$). This also calculated the SPI at different timescales (1, 3, 6, and 12 months). An SPI of ≤ -0.5 was defined as a dry event, and the number and intensity of droughts are calculated. The number of droughts was defined as the number of months and years of drought disasters. The drought intensity was the SPI monthly scale value for mild drought and above. The intensity of decadal drought in the study area was calculated as

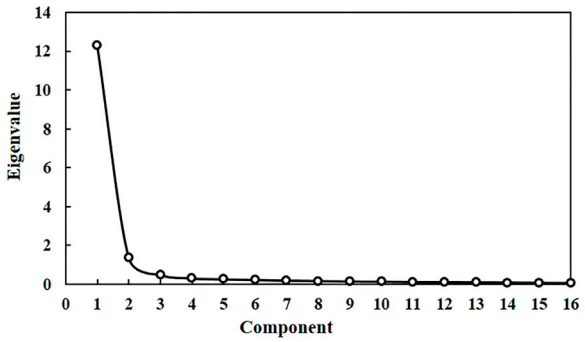

FIGURE 2
Results of principal component analysis.

the average of the aforementioned SPI values. Finally, the drought index was calculated using the observed precipitation series from the 16 meteorological stations, the regional series of homogeneous regions obtained by PCA, and the series for the entire WRB.

3.4 Standardized precipitation evapotranspiration index

The standardized precipitation evapotranspiration index (SPEI) proposed by Vicente-Serrano et al. (2010) is a drought index that considers both precipitation and evapotranspiration. Potential evapotranspiration (PET) is calculated according to Thornthwaite's method (Thornthwaite, 1948). By calculating the difference between monthly precipitation and potential evapotranspiration, the water deficit accumulation sequence is established. Then, the log-logistic probability distribution function is used to standardize the cumulative probability density, and the SPEI index is obtained. The SPEI dry events and drought categories are consistent with the SPI.

4 Results

4.1 Classification in the Weihe River basin based on monthly series

Figure 2 shows the PCA results of the monthly precipitation series based on 16 meteorological stations. We obtained two components with eigenvalues >1. Figure 3 indicates the spatial representativeness of these components. The spatial distribution pattern of factor loads was consistent, and the principal components do not overlap. Components 1 and 2 represent the northwestern and southeast regions, respectively.

Figure 4 shows the monthly precipitation classification of the WRB when applying the maximum loading rule. The northwestern region is large, including 10 meteorological stations (Minxian, Linyao, Huajialing, Huanxian, Pingliang, Xifengzhen, Guyuan, Xiji, Luochuan, and Wuqi). The southeast region is small, including six meteorological stations (Changwu, Wugong, Huashan, Foping, Shangzhou, and Zhen'an).

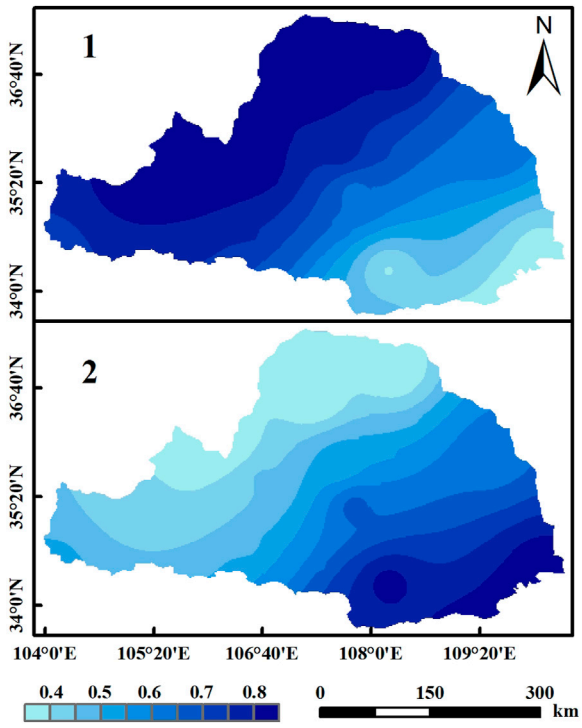

FIGURE 3
Spatial distribution of the principal components.

Once the homogeneous areas were identified, a regional precipitation series for each area was formed using the weighted averages of monthly precipitation records at each observatory. Similarly, a regional series for the WRB overall was created using the same procedure. The weight factor was the ratio of the surface area represented by each observatory to the total area of that region based on Thiessen's polygon method (Huang and Li, 1996; Jones and Hulme, 1996). The spatial representativeness of the regional precipitation series was consistent with the classified patterns. The correlation analysis between the two regional series and the precipitation series of the different observatories indicated that the regional series represented the evolution of the monthly precipitation of the homogeneous areas obtained from the PCA classification (Figure 5).

4.2 Drought evolution in different regions

Figure 6 shows the evolution of the SPI at the 6-month timescale in the two regions from 1970 to 2020. The number of occurrences of different drought classes was spatially inconsistent and decreased with higher classes. As shown in Table 1, more droughts were recorded in the northwest (193) and southeast (186) regions. In the northwest region, the drought was the most severe in the 1990s and the number of extreme droughts was the highest during this time, with no extreme droughts occurring in the 2000s and 2020s. In the southeast region, the drought intensity was highest in the 1990s, with the highest number of extreme droughts. No extreme droughts occurred in the 1970s, 1980s, and 2020s. In 2020, there was no

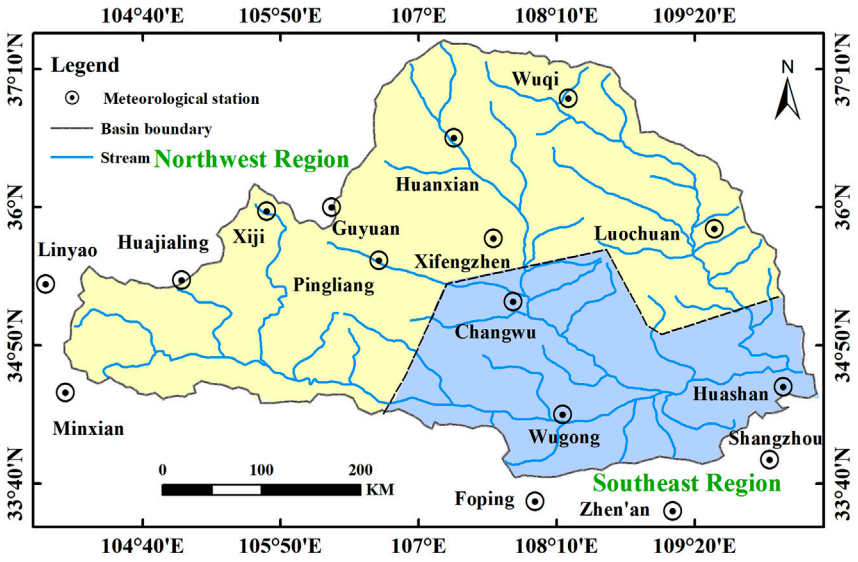

FIGURE 4
Spatial distribution of the meteorological stations.

drought in the northwest region, but moderate and severe drought occurred in the southeast region. The response time to drought in different regions was inconsistent because there was little or no rain for some time, and the precipitation is significantly less than in other periods, resulting in droughts not occurring at the same time (Zhang L. et al., 2022). In the 1990s, the WRB was most severely drought-stricken, and the frequency of drought in the northwest region was higher than in the southeast region.

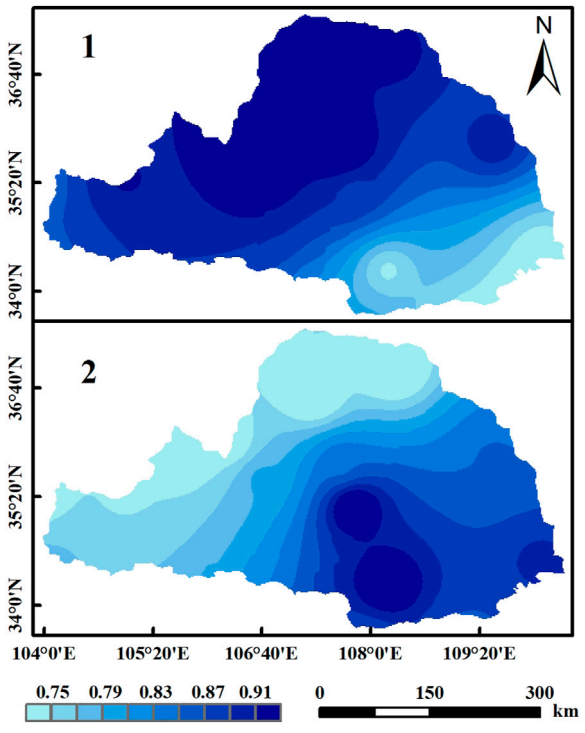

FIGURE 5
Correlation between the two regional series and monthly precipitation series in the different observatories.

4.3 Response of drought to El Niño/La Niña in the Weihe River basin

This study defined an El Niño/La Niña peak year of moderate intensity or higher as the event year; i.e., an El Niño/La Niña year, to explore the impact of ENSO on drought in the WRB. Figure 7 shows the multi-year mean SPI values at different timescales of El Niño/La Niña and the year following these events in the WRB. The SPI values were obtained from the regional precipitation series for the WRB. Figure 7 indicates the general drought response and significant differences (p<0.05) at different timescales when El Niño/La Niña occurred. As shown in Figure 7A, at a timescale of 1 month, a negative average SPI value was observed in July during El Niño years. The July of El Niño years showed significant differences compared to the rest of the years, the normal years, and the La Niña years. During El Niño years, negative average SPI values were recorded for July and November at the 3-month timescale; moreover, >78% of SPI values from August to November were negative. Significant drought (SPI/SPEI ≤ −0.5 and p < 0.05) only occurred in September compared to other years and normal years. At the 6-month timescale, negative average SPI values occurred from July in the El Niño year to February of the following year. Moreover, >78% of SPI values from August to December and February of the following year were negative. These figures were significant in November and December between El Niño and the rest of the years. The multi-year average SPI values from March to December of the following year were positive, and there were significant humid conditions from August to October and December compared to La Niña. However, at longer timescales (12 months), the number of significant drought months increased, and El Niño years showed significant droughts in January, April, and

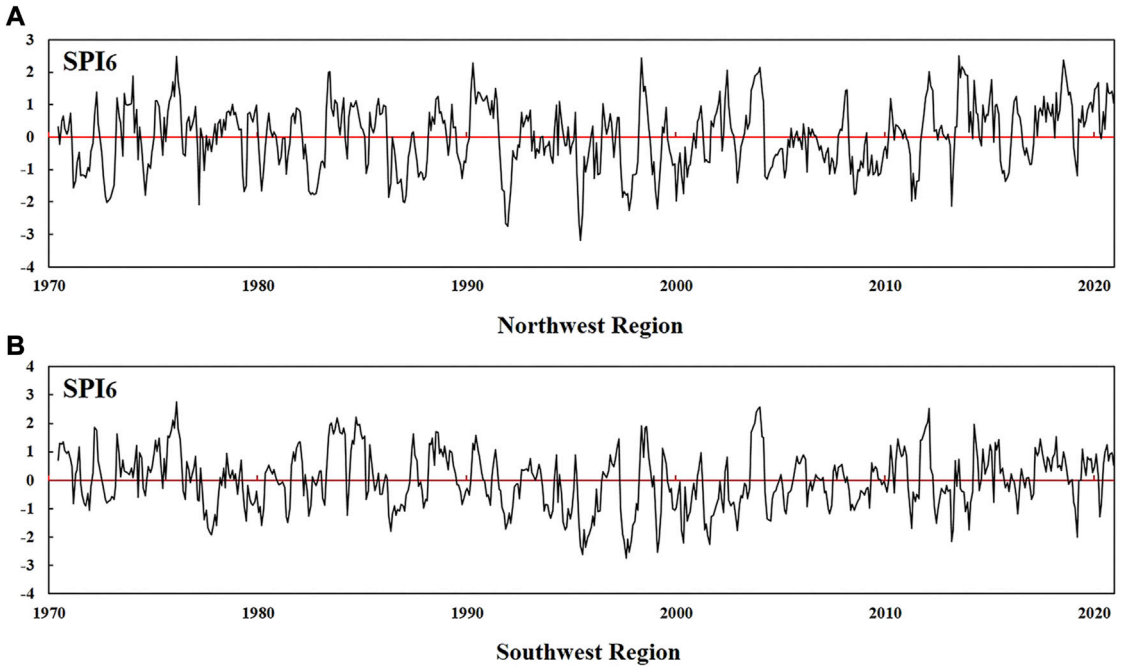

FIGURE 6
Evolution of SPI series at a 6-month timescale obtained from the two regional precipitation series. **(A)** Northwest Region. **(B)** Southwest Region.

TABLE 1 Numbers of drought occurrences in different regions.

	Mild drought	Moderate drought	Severe drought	Extreme drought
Northwest Region	85	62	34	12
Southeast Region	89	55	29	13

September and June of the following year compared to normal years and other years. The average SPI values from August to December in the year following El Niño were positive, with no significant differences in December compared to La Niña years. The longer the timescale of SPI, the more months of significant drought in El Niño years and the year following El Niño, while the intensity of drought weakened.

On different timescales in the WRB, El Niño and La Niña showed different effects on the SPI index. As shown in Figure 7B, at a timescale of 1 month, the average SPI values in February, November, and December of the following year were positive. These months differed significantly from other years, normal years, and El Niño years and were significantly humid. Significant droughts were observed in June and July of the following year. At the 3-month timescale, the multi-year average SPI values of La Niña from May to September of the following year were negative, and 71% of the SPI values from May to August were negative, indicating significant droughts in July and August compared to normal years and El Niño years. At the 6-month timescale, >71% of the SPI values from July to November in El Niño years were negative. Significant differences were observed between La Niña and other years and between normal years and El Niño years in July and August. At the 12-month timescale, no significant difference was observed between La Niña and other years and normal years. Significant differences were observed between La Niña and El Niño years only in August and October. On different timescales, La Niña had a stronger drought the following year than El Niño the following year. At the 3-, 6-, and 12-month timescales, as the timescale increased, La Niña intensified the drought in the following year, with the worst summer droughts. At the 12-month timescale, La Niña had less impact on drought than El Niño. The response of SPI12 (SPI at the 12-month timescale) to El Niño in the WRB was significant, with 25% of months experiencing significant drought. The remaining timescales show fewer months of significant drought. The responses of SPI3 (SPI at the 3-month timescale) and SPI6 (SPI at the 6-month timescale) to La Niña were significant, and both showed significant droughts in July and August of the next year. Short-term drought events were strongly associated with La Niña.

At a timescale of 1 month, the WRB experienced significant drought (SPI) in July of El Niño years, November of the year following El Niño, and June of the year following La Niña. Significant droughts (SPEI) occurred in June of the year following La Niña. At the 3-month timescale, significant

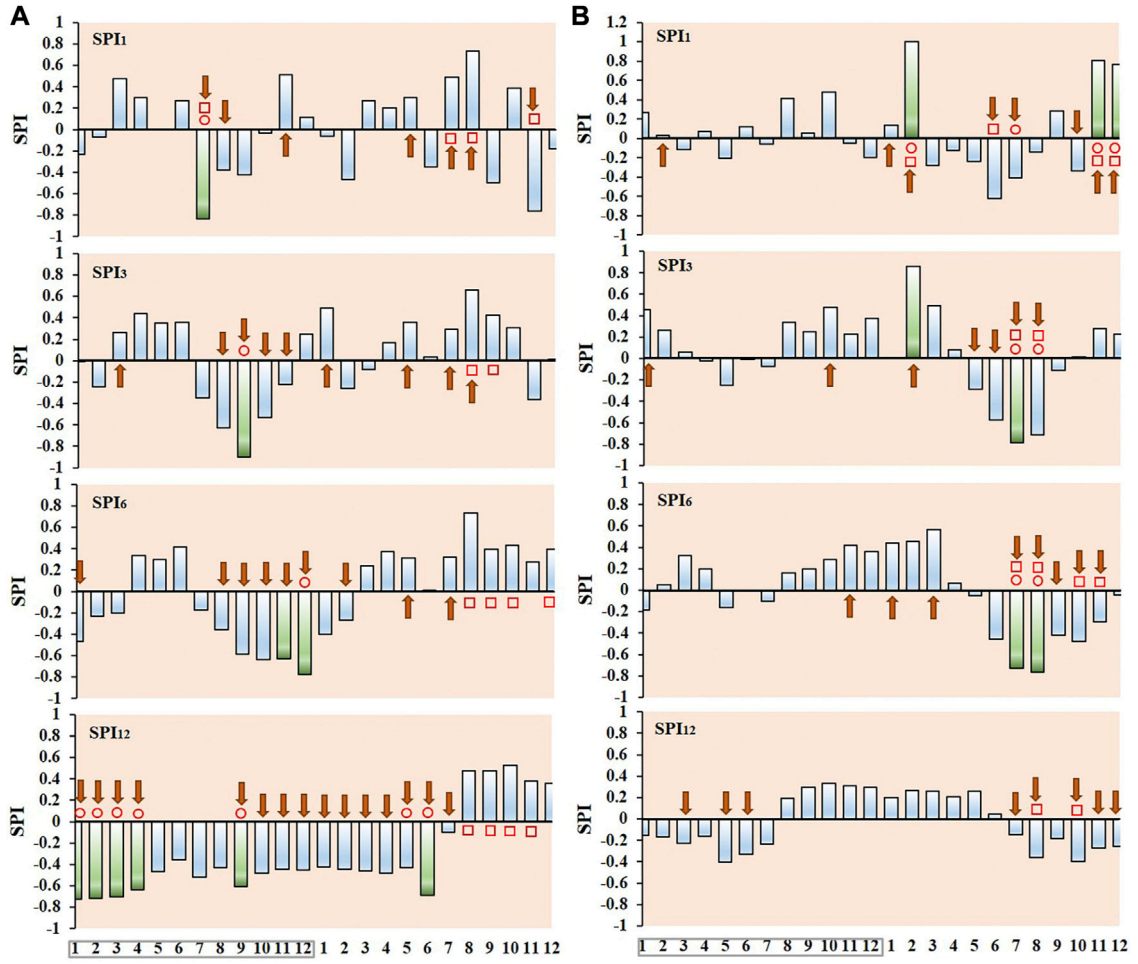

FIGURE 7
Mean SPI values at different timescales from the SPI series in the Weihe River basin. **(A)** El Niño and **(B)** La Niña years (boxed) and the year after these events. Green columns, significant differences in SPI values between El Niño/La Niña and the remaining years; blue columns, no significant difference; square, significant differences in SPI values between El Niño and La Niña years; circles, significant differences in SPI values between El Niño/La Niña years and normal years; arrows, months with consistent anomalies among events [>70% of events have the same sign as the mean SPI (Vicente-Serrano, 2005)].

droughts (SPI and SPEI) occurred in September of El Niño years and July of the year following La Niña. The SPEI showed significant droughts in September of El Niño years and July of the year following La Niña. At the 6-month timescale, significant droughts (SPI) occurred in November and December of El Niño years and July and August of the year following La Niña. No significant droughts occurred by SPEI. At the 12-month timescale, the trends of SPI and SPEI values were the same, with no significant droughts in La Niña years and the year following La Niña (Figure 7; Supplementary Figure S1).

As shown in Figure 8, the highest percentages of years with drought were 44% in El Niño years, 43% in the year following La Niña, and 38% in the year following La Niña years. The smallest percentages were observed in the year following El Niño (22%). Different categories of drought occurred differently according to the event. Extreme and severe droughts occurred only in El Niño years and the following year, while mild droughts occur most frequently in different events.

Figure 9 shows the percentage of the WRB that were significantly dry during El Niño and La Niña years. During El Niño years, analysis of the differences between El Niño years and the rest of the years (normal and La Niña years) (Figure 9A) showed that parts of the WRB were affected by significant drought. More than 13% of the total surface was affected between September of the El Niño year and February of the following year. Moreover, during December of the El Niño year, significant dry conditions occurred in a high percentage of the area (45%). Analysis of the significant dry conditions between El Niño and the normal years (Figure 9B) showed that the area of drought decreased in December and increased in January and February of the following year. The consistent surface areas between July of the El Niño year and February of the following year were 13%–51% (Figure 9C).

The proportions of significant drought areas in the year following La Niña were higher than those during La Niña years, which was related to decreased precipitation in the following year. During La Niña years, significant dry conditions were recorded in 5% to 32% of the WRB between July and February of the following year, based on differences

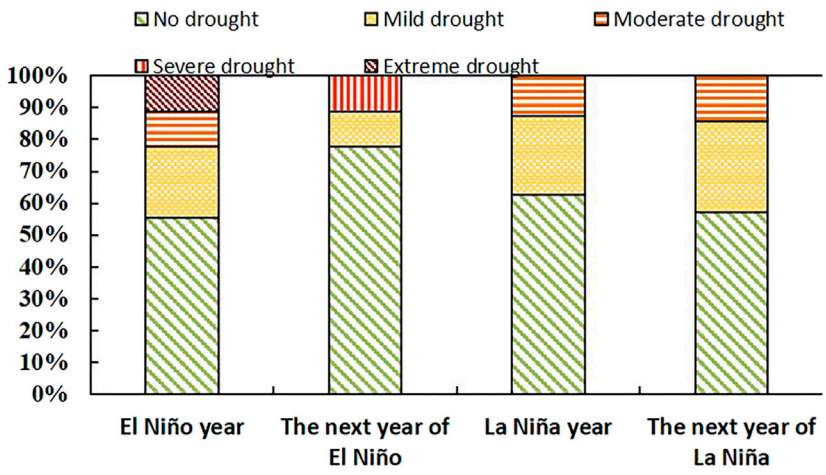

FIGURE 8
Percentages of drought years in El Niño/La Niña and the following year.

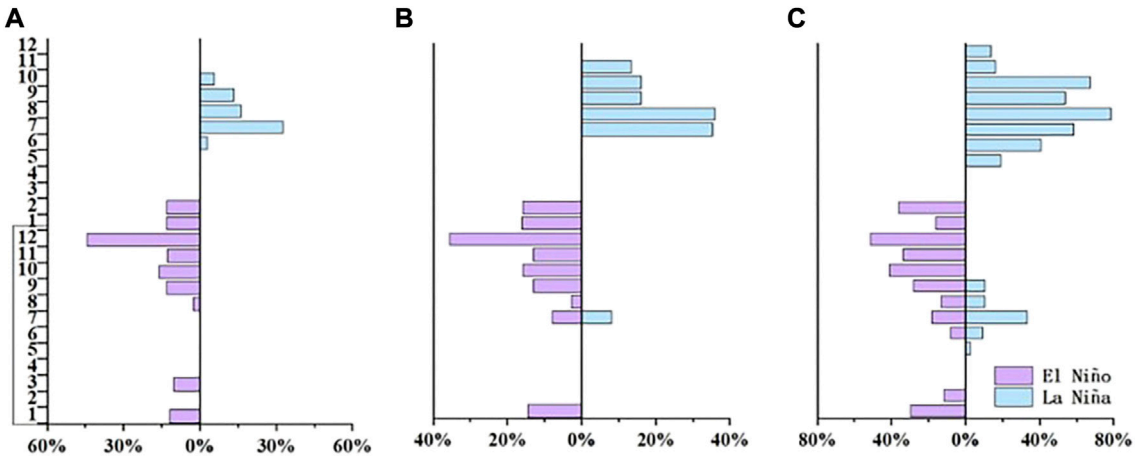

FIGURE 9
Percentage of the Weihe River basin, during El Niño/La Niña (boxed), and the following year, with significant drought areas in the 6-month SPI between **(A)** El Niño/La Niña and the remaining years and **(B)** El Niño/La Niña and normal years. **(C)** Percentage of the Weihe River basin with consistently negative anomalies among events during El Niño and La Niña years.

between La Niña and the rest of the years. The analysis of the differences between La Niña and normal years in these months showed obvious increases in significant drought areas. However, the La Niña signal was very consistent, with >54% of the area having a negative mean SPI value. Droughts mainly occurred at the end of El Niño years and the beginning of the following year, and in the year following La Niña.

4.4 Spatial differences in the influence of El Niño/La Niña on drought conditions in the Weihe River basin

Here, the spatial differences presented by the SPI averages at the various timescales during the El Niño and La Niña years are described from the regional series of the two homogeneous regions obtained from PCA. Figure 10 shows the average SPI values according to the different timescales during El Niño and La Niña for the northwestern region. Figure 10A demonstrates that >78% of SPI values from July to September were negative on a 1-month timescale in El Niño years. El Niño years showed significant differences only in July compared to the rest of the years, normal years, and La Niña years. At the 3-month timescale, >78% of SPI values from August to November were negative. El Niño years showed significant droughts from August to October compared to the rest of the years, with significant differences only in September compared to normal years. The drought pattern intensified on a 6-month timescale, with September to December showing significant droughts

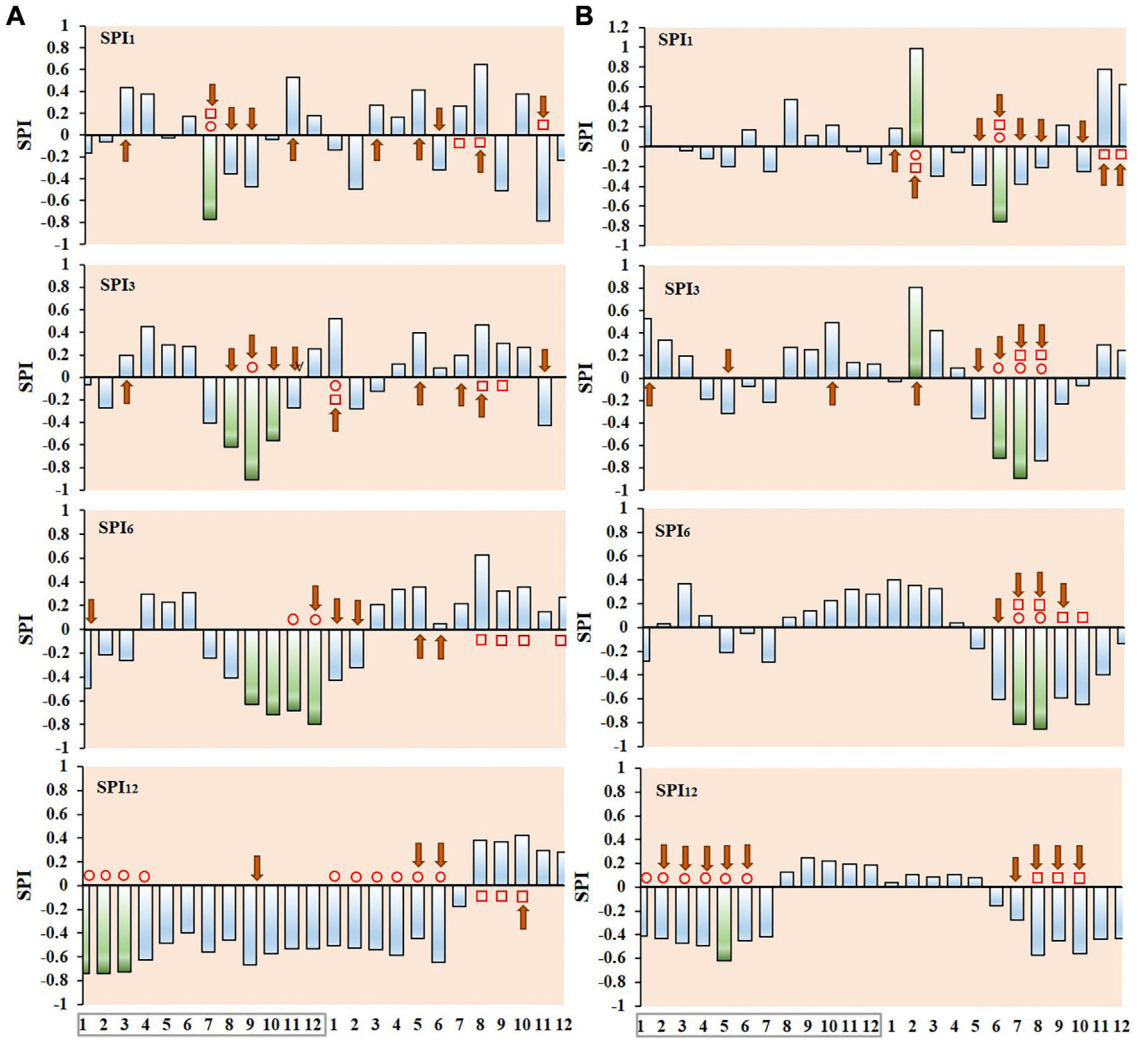

FIGURE 10
Mean SPI values at different timescales from SPI series in the northwest region. **(A)** El Niño and **(B)** La Niña years (boxed) and the year after these events. Same as Figure 7.

compared to the rest of the years. The year following El Niño showed significant humidity from August to October and December. Significant droughts were recorded from January to April of El Niño years and from January to April of the following year at the timescale of 12 months but only compared to the normal years.

The temporal patterns were reversed during La Niña, with fewer months showing significant differences. As shown in Figure 10B, at a timescale of 1 month, February and June of the following year in La Niña differed significantly from the rest of the years, the normal years, and the El Niño years, with February significantly wetter and June significantly drier. At the 3-month timescale, >71% of SPI values for the year following La Niña were negative from May to August, with June to August (summer) showing significant droughts. At the 6-month timescale, between August of La Niña years and April of the following year, the average SPI values were positive. The following year, the mean SPI values were negative from May to December, with significant differences from July to October compared to El Niño and only in July and August compared to the rest of the years and the normal years. On a 12-month timescale, La Niña year shows significant droughts in May compared to normal years and significant differences from August to October of the following year compared to El Niño years.

Figure 11 shows the mean SPI values at different timescales during El Niño and La Niña in the southeast region. The mean SPI values were higher than those in the northwest region at different timescales and the number of months with significant differences was less than that in the northwest region. As shown in Figure 11A, at a timescale of 1 month, only July in El Niño showed significant droughts, and >78% of the SPI values were negative. At the 3-month timescale, >78% of the SPI values were positive from March to June in El Niño years, with the following August to September showing significant dampness compared to La Niña years. At timescales of 6 and 12 months, no significant anomalies were recorded in relation to El Niño and La Niña years, although significant differences were observed between the year following

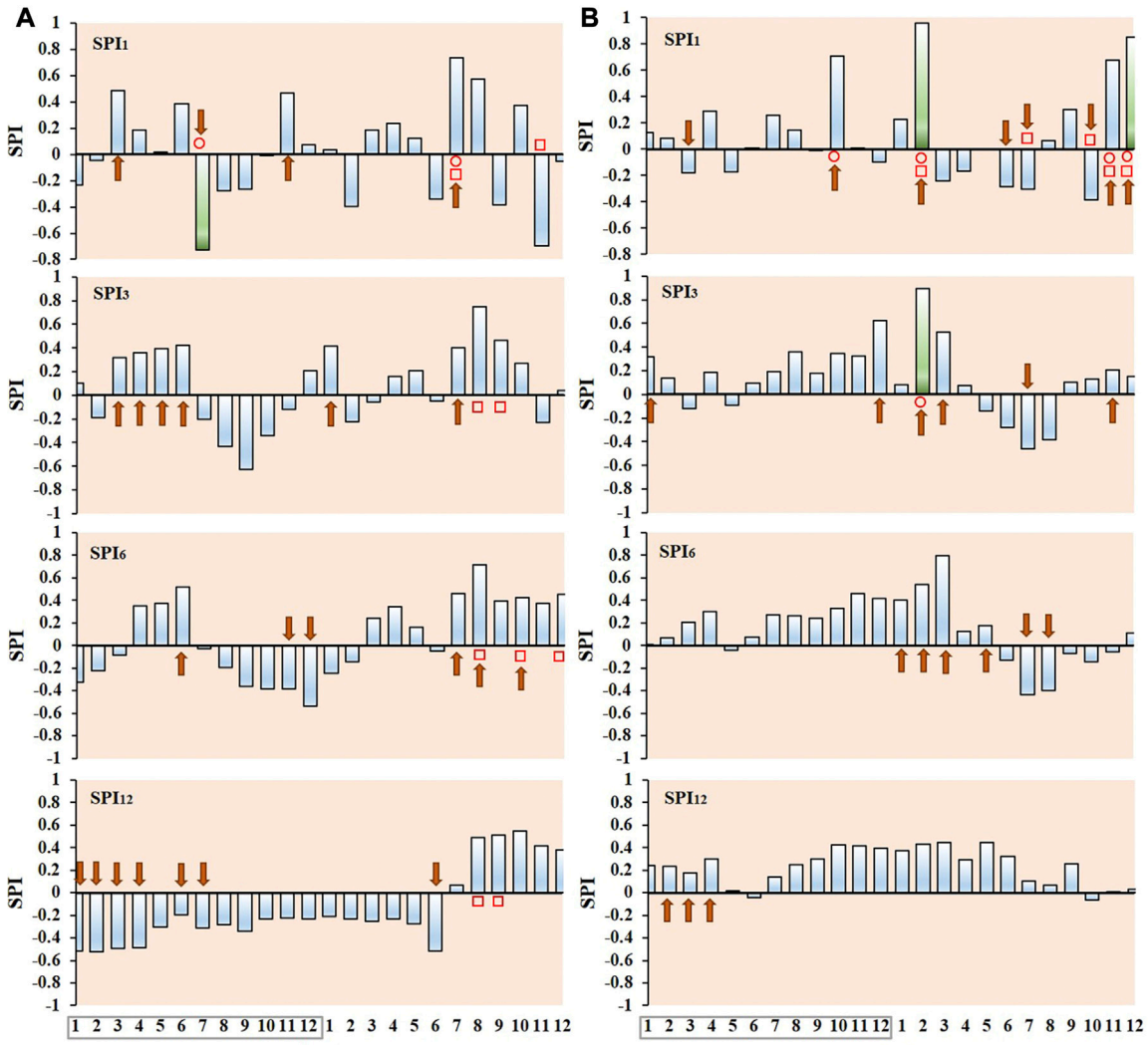

FIGURE 11
Mean SPI values at different timescales from SPI series in the southeast region. **(A)** El Niño and **(B)** La Niña years (boxed) and the year after these events. Same as Figure 7.

El Niño and the La Niña year only for a few months of the following year.

As shown in Figure 11B, at the 1-month timescale, February, November, and December of the following year in La Niña differed significantly from the normal years and El Niño years. At the 3-month timescale, February of the following year differed significantly from the rest of the years and the normal years, showing significant wetness. No significant anomalies were recorded in relation to El Niño and La Niña events at the 6- and 12-month timescales.

El Niño and La Niña had greater impacts on the drought index in the northwest of the WRB, with more months of significant drought and greater intensity levels in the northwest compared to the southeast. The negative anomalies were stronger in El Niño years than in La Niña years, with different months of significant drought in different regions. The northwest SPI12 showed significant responses to El Niño, with 38% of months experiencing significant drought, while the SPI6 responded significantly to La Niña, with 17% of months experiencing significant drought. The southeast experienced significant droughts in July of El Niño years only on the 1-month timescale.

At the 1-month timescale, the northwest region experienced significant droughts (SPI and SPEI) in July of El Niño years and June of the year following La Niña. At the 3-month timescale, significant droughts (SPI) occurred from August to October in El Niño years and from June to August in the year following La Niña. The SPEI showed significant droughts in September of the El Niño year and July and August of the year following La Niña. At the 6-month timescale, significant droughts (SPI and SPEI) occurred in September and November of El Niño years and October of the year following La Niña. At the 1-, 3-, and 6-month timescales, the longer the SPI and SPEI timescale, the later the significant droughts occurred. At the 12-month timescale, SPI and SPEI showed significant droughts in April in El Niño years (Figure 10; Supplementary Figure S2). At the 1-month timescale, the southeast region experienced significant drought (SPI) in July of El Niño years and November of the year following El Niño. No

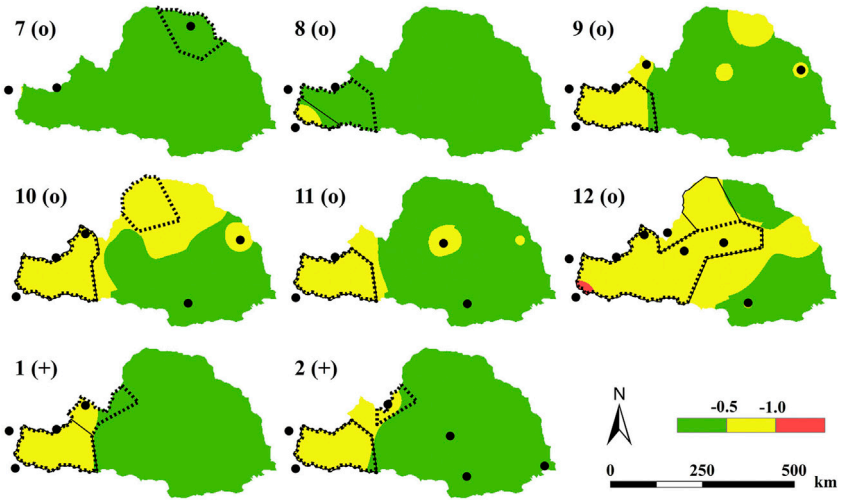

FIGURE 12
Spatial distribution of SPI6 averages from July of El Niño years (open circles) to March of the following year (pluses). Area within the black solid line, significant difference between the El Niño years and the remaining years, showing significant drought; area within the black dashed line, significant difference between El Niño and normal years, showing significant drought; solid circles, observatories with consistent anomalies among El Niño events.

significant droughts occurred by SPEI. At the 3-, 6-, and 12-month timescales, no significant droughts (SPI and SPEI) occurred in the southeastern region (Figure 11; Supplementary Figure S3).

The areas with significant changes in negative averages differed during the various months of El Niño and La Niña. The mean SPI values obtained from SPI series from different meteorological stations on a 6-month timescale showed that most of the WRB was affected by drought between July of El Niño years and February of the following year and from May to December in the year following La Niña. Figure 12 and Figure 13 show areas with significant differences between the corresponding El Niño/La Niña and the rest of the years (inside the black line), areas with significant differences between El Niño/La Niña and normal years (inside the black dashed line), and the meteorological stations with consistency among events.

As shown in Figure 12, the areas of significant drought were higher in the northwest than in the southeast region from August of El Niño years to February of the following year. From September to November in El Niño years, a high percentage of the northwest region showed significant drought between El Niño and the rest of the years and the normal years. From December of El Niño to February of the following year, the areas of significant drought decreased. December of El Niño years showed larger areas of significant drought compared to the rest of the years, but a smaller area compared to El Niño and normal years. January and February of the year following showed opposite trends of those for December. Event consistency was recorded at 50% of the meteorological stations in December and at a few meteorological stations in the remaining months.

The southeast region was not affected by significant droughts during the year following La Niña (between La Niña and the rest of the years and between La Niña and normal years). As shown in Figure 13, no droughts occurred in the southeast region in May and June. Significant drought conditions were recorded in the northwest region from July to November of the year following La Niña, indicating significant drought conditions between La Niña and normal years. La Niña resulted in smaller areas of significant drought compared to the rest of the years. Many meteorological stations showed consistency in recorded events compared to El Niño years.

5 Discussion

The main objective of this study was to study the effects of ENSO on meteorological drought in the WRB through the classification of meteorological stations. We compared the effects of El Niño and La Niña on drought. Zhao et al. (2018) reported that ENSO is significantly related to meteorological and hydrological droughts in the WRB. Gore et al. (2020) found that El Niño (La Niña) conditions weaken (strengthen) the Walker circulation, causing drier (wetter) conditions over parts of southern Africa. These studies on the impact of ENSO on drought mostly focused on the whole region. Sun et al. (2015) analyzed the drought zoning, drought characteristics, and drought frequency in northeast China based on PCA. Wang et al. (2017) studied the drought trends and characteristics of periodic variation at multiple timescales in different regions. The present study refined the analysis of the influence of El Niño/La Niña on drought by dividing the WRB. The results showed that the northwest and southeast regions respond differently to ENSO. These results improve the understanding of the mechanism by which ENSO affects droughts and inform the development of a drought warning system.

As shown in Supplementary Figure S4A, in El Niño years, the average annual precipitation in the northwest region of has 66.4 mm and 51.2 mm less than the following year and the normal year. La Niña year received more precipitation (519.8 mm) than in the

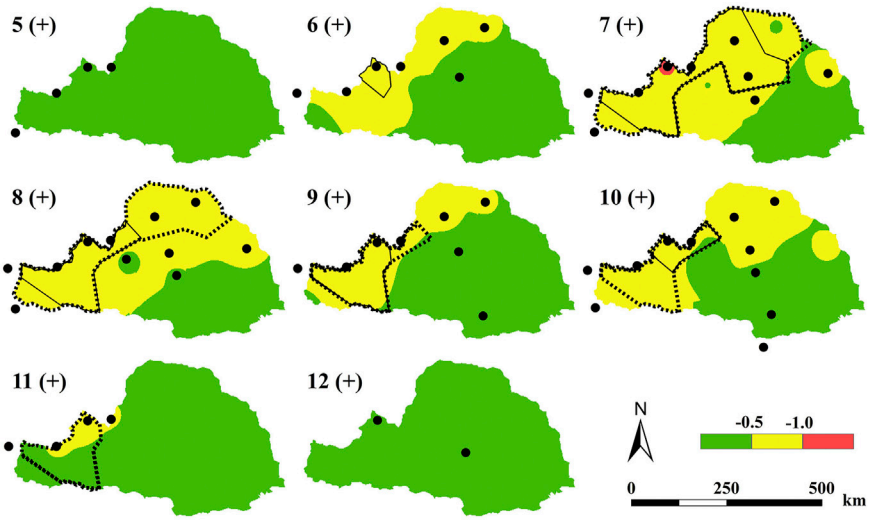

FIGURE 13
Spatial distribution of SPI6 averages for different months from May to December for the year after La Niña (pluses). Same as Figure 12.

following year (466.7 mm) and in the normal year (512.0 mm), but more precipitation in the normal year than in the following year. The El Niño annual precipitation (616.0 mm) in the southeast region is less than that in the following year and normal year, but the precipitation in the following year (696.6 mm) is more than that in the normal year (637.9 mm), which is consistent with the situation in the northwest region. The precipitation in La Niña year is 41.7 mm and 52.9 mm more than that in the following year and normal year. The normal annual precipitation was 5.8 mm lower than the year following La Niña.

As shown in Supplementary Figure S4B, the highest temperature in the northwestern region was 7.7°C in El Niño years, followed by 7.6°C in the following year, and the lowest in normal years. Temperatures in La Niña years (7.6°C) were lower than in El Niño years. The temperatures in La Niña years were higher than the following year and normal years, while the temperatures in the following year (7.3°C) were lower than normal (7.6°C). Temperature was generally higher in the southeast region than in the northwest region. El Niño and La Niña years were both warmer than the following year. Temperatures in El Niño and the following year were higher than those in normal years, while temperatures in La Niña year and the following year were lower than those in normal years.

Comparison of El Niño years with normal years revealed that 91% of regions in the WRB showed decreasing trends in precipitation and 95% of the regions showed increasing trends in temperature (Supplementary Figure S4C). Compared with the next year, the precipitation in the year following El Niño was higher than that in El Niño, and 94% of the regions showed decreasing trends in temperatures. Comparing La Niña years with normal years, 55% of the regions showed an increasing trend in precipitation, while 72% of the regions showed a decreasing trend in temperature. Comparing La Niña year with the following year, 98% of the regions showed a decreasing trend in precipitation in the following year. The temperature in the year following in La Niña was lower than that in La Niña. El Niño had a decreasing effect on precipitation while La Niña had an increasing effect on precipitation, consistent with the results of the precipitation in the WRB under the influence of ENSO reported by Zhao et al. (2018). The temperatures rose in El Niño years, consistent with Su's analysis of high-temperature weather in the north under the influence of ENSO (Su et al., 2022).

Wang et al. (2022) observed a northerly wind anomaly during El Niño, resulting in a weak northward transport of water vapor from the South China Sea and the Bay of Bengal, and less precipitation in northern China. Wu et al. (2017) reported unusually high precipitation due to an anticyclonic circulation in the northwest Pacific Ocean and an anomalous double-blocking circulation in the year following El Niño. This finding can be explained by the drought in the WRB mainly occurring in El Niño years, in which the next year was generally wet. The influence of El Niño on precipitation in northern China may be related to the strength of summer monsoons. When El Niño is strong, the monsoons affecting northern China are weak in summer and autumn, resulting in low annual precipitation in El Niño years and high precipitation in summer and autumn in La Niña years (Jia and Zhang, 2020). Therefore, SPI12 responded significantly to El Niño, and droughts in short timescales were closely related to La Niña (Wang et al., 2021).

We calculated SPEI at different timescales (1, 3, 6, and 12 months) in the WRB and the northwest and southeast regions. The mean SPEI values at different timescales in El Niño/La Niña years and the next year are shown in Supplementary Figures S1–S3. At 1-, 3-, and 6-month timescales, the impact of El Niño/La Niña years on SPEI was consistent with the following year. Few months differed significantly between El Niño/La Niña and normal years and the rest of the year. SPEI cannot show differences between the effects of El Niño and La Niña on drought, or the differences in the El Niño/La Niña effects on drought from the following year. On the 12-month timescale, the effects of El Niño/La Niña and its next year on SPEI differed. Drought mainly occurred in El Niño years, while no drought occurred in La Niña years and the following year. The response of SPEI to El Niño and La Niña is not as strong as for

SPI, which is consistent with the findings of Wang et al. (2021). According to Zhao et al. (2017), Walker circulation significantly impacts precipitation in China. Weakened circulation leads to decreased precipitation in northern China and may cause drought. Bayr et al. (2014) found that ENSO affects precipitation in northern China by influencing the intensity of Walker circulation. In summary, ENSO affects the SPI index of the WRB by influencing precipitation and, thus, drought in the WRB, consistent with the findings of Li et al (2019).

During the La Niña period, due to the cold water anomaly in the equatorial eastern Pacific, the equatorial easterly wind increased and the Hadley circulation weakened (Kong et al., 2021). The western Pacific subtropical high weakened and moved northward (Xue and Zhao, 2017). The rain belt also moved northward (Zhang et al., 2023). El Niño can cause atmospheric Gill-type responses through anomalous Walker circulation, making the western Pacific subtropical high stronger and move westward and southward (Qian et al., 2018). The northwest area of the WRB is far from the ocean and the transfer of water vapor gradually decreases from the southeast to the northwest. The precipitation in the northwest is lower than that in the southeast (Yang et al., 2023). In general, the northwest region had a significantly higher number of months with significant drought compared to the southeast region. This finding is consistent with the report by Huang et al. (2015) of a higher probability of drought in the northwest compared to the southeast.

6 Conclusion

We assessed the impact of El Niño and La Niña on drought from 1970 to 2020 in the WRB in China using standardized precipitation indices at different timescales. The conclusions are as follows.

(1) In the 1990s, the most severe drought occurred in the WRB, with more droughts occurring in the northwest region than in the southeast. El Niño/La Niña have different levels of impact on drought in the WRB, with the highest number of drought years occurring in El Niño years, followed by the following year of La Niña.
(2) The number of months with significant drought increased but the drought intensity weakened in the WRB as the timescale of SPI increases. At the timescales of 3 and 6 months, the summer drought in the following year of La Niña was the most severe. At the 12-month timescale, La Niña had a lower impact on drought than El Niño.
(3) The effects of drought in El Niño and La Niña were spatially inconsistent. On different timescales, significant high-intensity droughts were recorded in the northwest region. Significant droughts existed in southeast region in July of El Niño years at the 1-month timescale (SPI).

Data availability statement

The original contributions presented in the study are included in the article/Supplementary Material; further inquiries can be directed to the corresponding authors.

Author contributions

JF, SW, and DL contributed to the study conception and design. DL, TQ, and YC organized the database. SW performed the statistical analysis. SW wrote the first draft of the manuscript. FX, CW, and GL wrote sections of the manuscript. All authors contributed to manuscript revision and read and approved the submitted version. All authors contributed to the article and approved the submitted version.

Funding

This research was funded by the National Natural Science Foundation of China (grant number 52209013), Department of Education of Hebei Province (grant number ZD2022085), State Key Laboratory of Eco-hydraulics in Northwest Arid Region (grant number 2019KFKT-4), and National Natural Science Foundation of China (grant number 52009053).

Conflict of interest

The authors declare that the research was conducted in the absence of any commercial or financial relationships that could be construed as a potential conflict of interest.

Publisher's note

Supplementary material

The Supplementary Material for this article can be found online at: https://www.frontiersin.org/articles/10.3389/feart.2023.1093632/full#supplementary-material

References

Arslan, O. (2009). A GIS-based spatial-multivariate statistical analysis of water quality data in the Porsuk River, Turkey. *Water Qual. Res. J.* 44 (3), 279–293. doi:10.2166/wqrj.2009.029

Badakhshan Farahabadi, F., Fathi Vajargah, K., and Farnoosh, R. (2021). Dimension reduction big data using recognition of data features based on copula function and principal component analysis. *Adv. Math. Phys.* 2021, 1–8. doi:10.1155/2021/9967368

Bayr, T., Dommenget, D., Martin, T., and Power, S. B. (2014). The eastward shift of the Walker Circulation in response to global warming and its relationship to ENSO variability. *Clim. Dynam.* 43 (9), 2747–2763. doi:10.1007/s00382-014-2091-y

Bjerknes, J. (1969). Atmospheric teleconnections from the equatorial Pacific. *Mon. Wea. Rev.* 97 (3), 163–172. doi:10.1175/15200493(1969)097<0163:ATFTEP>2.3.CO;2

Chang, J., Wang, Y., Istanbulluoglu, E., Bai, T., Huang, Q., Yang, D., et al. (2015). Impact of climate change and human activities on runoff in the Weihe River Basin, China. *Quatern. Int.* 380, 169–179. doi:10.1016/j.quaint.2014.03.048

Dai, A. (2013). Increasing drought under global warming in observations and models. *Nat. Clim. Change* 3 (1), 52–58. doi:10.1038/NCLIMATE1633

Dai, M., Huang, S., Huang, Q., Zheng, X., Su, X., Leng, G., et al. (2022). Propagation characteristics and mechanism from meteorological to agricultural drought in various seasons. *J. Hydrol.* 610, 127897. doi:10.1016/j.jhydrol.2022.127897

Feng, J. D., Liu, S. Y., Xie, Y. Y., Huang, C. J., and Shen, T. (2022). Spatio-temporal variations of inhomogeneous distribution of precipitation in the Wei River Basin. *J. China. Hydrol.* 42 (02), 85–90. doi:10.19797/j.cnki.1000-0852.20210135

Gao, Y. L., Liu, X. G., Leng, X. X., Zhang, Y. Y., Dong, J. H., and Fan, C. (2020). Spatio-temporal drought patterns in Guangxi Province based on principal component analysis. *Acta. Ecol. Sin.* 16, 5591–5601.

Gore, M., Abiodun, B. J., and Kucharski, F. (2020). Understanding the influence of ENSO patterns on drought over southern Africa using SPEEDY. *Clim. Dynam.* 54 (1-2), 307–327. doi:10.1007/s00382-019-05002-w

Guo, A. J., Chang, J. X., Huang, Q., and Sun, J. N. (2014). Quantitative analysis of the impacts of climate change and human activities on runoff change in Weihe Basin. *J. Northwest A F Univ. Nat. Sci. Ed.* 42 (08), 212–220. doi:10.13207/j.cnki.jnwafu.2014.08.024

He, Y., Wang, F., Mu, X. M., Bai, H., Jiang, C., and Li, R. (2012). Temporal and spatial characteristics of temperature and precipitation in Weihe River Basin. *Bull. Soil Water Conserv.* (04), 102–105. doi:10.13961/j.cnki.stbctb.2012.04.010

Hu, J., Li, P., Zhao, G., Mu, X., Hörmann, G., Gao, P., et al. (2022). Effects of climate variability and anthropogenic factors on sediment load reduction in the Weihe River basin, China. *Hydro. Process.* 36 (4), e14562. doi:10.1002/hyp.14562

Huang, B., and Li, R. R. (1996). Thiessen polygon and its application in calculating the biomass of any depth contour. *Remote Sens. Tech. Appl.* 03, 36–40.

Huang, S. Z., Huang, Q., Wang, Y. M., and Chen, Y. T. (2015). Evolution of drought characteristics in the Weihe River Basin based on standardized precipitation index. *J. Nat. Disasters.* 24 (1), 15–22. doi:10.13577/j.jnd.2015.0103

Ipcc (2018). *Global warming of 1.5°C (Special report)*. Cambridge, UK: Cambridge University Press.

Ipcc (2021). "Summary for policymakers," in *Climate change 2021: The physical science basis. Contribution of working group I to the sixth assessment report of the intergovernmental panel on climate change* (Cambridge, UK: Cambridge University Press). In Press.

Ipcc (2022). "Summary for policymakers," in *Climate change 2022: Impacts, adaptation, and vulnerability. Contribution of working group II to the sixth assessment report of the intergovernmental panel on climate change* (Cambridge, UK: Cambridge University Press). In Press.

Jia, Y. Q., and Zhang, B. (2020). Correlation analysis of variation of dry-wet climate and ENSO in Northern China during 1960-2017. *Sci. Geogr. Sin.* 40 (12), 2115–2124. doi:10.13249/j.cnki.sgs.2020.12.018

Jim´enez-donaire, M. P., Tarquis, A., and Gir´aldez, J. V. (2019). Evaluation of a combined drought indicator and its predictive potential for agricultural droughts in Southern Spain. *Nat. Hazards Earth Syst. Sci. Discuss.* 2018, 1–22. doi:10.5194/nhess-2019-135

Jones, P. D., and Hulme, M. (1996). Calculating regional climatic timeseries for temperature and precipitation: Methods and illustrations. *Int. J. Climatol.* 16, 361–377. doi:10.1002/(sici)1097-0088(199604)16:4<361:aid-joc53>3.0.co;2-f

Kim, S., and Kug, J. S. (2018). What controls ENSO teleconnection to east asia? Role of Western North Pacific precipitation in ENSO teleconnection to east asia. *J. Geophys. Res. Atmos.* 123 (18), 10–406. doi:10.1029/2018JD028935

Kong, Z. Y., Zhou, Y. H., Xu, X. Q., and An, X. R. (2021). Corelation analyses among ALOD.AAM and ENSO, and the 220-2021 La Nina event. *Prog. Astron* 29 (4), 532–543.

Kug, J. S., An, S. I., Ham, Y. G., and Kang, I. S. (2010). Changes in El Niño and La Niña teleconnections over North Pacific–America in the global warming simulations. *Theor. Appl. Climatol.* 100 (3), 275–282. doi:10.1007/s00704-009-0183-0

Kug, J. S., Jin, F. F., and An, S. I. (2009). Two types of El Niño events: Cold tongue El Niño and warm pool El Niño. *J. Clim.* 22 (6), 1499–1515. doi:10.1175/2008JCLI2624.1

Li, C., Zhang, H., Gong, X., Wei, X., and Yang, J. (2019a). Precipitation trends and alteration in Wei River Basin: Implication for water resources management in the transitional zone between plain and Loess Plateau, China. *China. Water* 11 (11), 2407. doi:10.3390/w11112407

Li, P., Huang, S. Z., Huang, Q., Wang, H., Wang, L., and Han, L. (2019b). Spatiotemporal characteristics of the formation and development of agricultural drought in Weihe River basin under changing environment. *J. Nat. Disaster.* 28 (4), 131–141. doi:10.13577/j.jnd.2019.0414

Liu, Y. G., Bao, J. C., Yang, Y. X., and Huang, X. (2022). Temporal and spatial characteristics of precipitation and evaporation in the Weihe River Basin from 1850 to 2005. *Res. Soil Water Conserv* (06), 224–232. doi:10.13869/j.cnki.rswc.2022.06.012

Luo, G. Y. (2020). A general survey of the studies on El Niño and La Niña in China. *Sci. Geogr. Sin.* 20 (3), 264–269.

Ma, C. H., Huang, S. Z., and Huang, Q. (2022). Dynamic change and driving force analysis of hydrological drought duration-severity dependency structure in the Weihe River Basin. *J. H. E.* 10, 1180–1193. doi:10.13243/j.cnki.slxb.20210961

Ma, S., Zhu, C., and Liu, J. (2020). Combined impacts of warm central equatorial Pacific sea surface temperatures and anthropogenic warming on the 2019 severe drought in East China. *Adv. Atmos. Sci.* 37 (11), 1149–1163. doi:10.1007/s00376-020-0077-8

Ma, Z. G., and Ren, X. B. (2007). Drying trend over China from 1951 to 2006. *Clim. Chang. Res.* (04), 195–201.

Markonis, Y., Kumar, R., Hanel, M., Rakovec, O., Máca, P., and AghaKouchak, A. (2021). The rise of compound warm-season droughts in Europe. *Sci. Adv.* 7 (6), eabb9668. doi:10.1126/sciadv.abb9668

Okumura, Y. M. (2019). ENSO diversity from an atmospheric perspective. *Curr. Clim. Chang. Rep.* 5 (3), 245–257. doi:10.1007/s40641-019-00138-7

Peng, J., Dadson, S., Hirpa, F., Dyer, E., Lees, T., Miralles, D. G., et al. (2020). A pan-African high-resolution drought index dataset. *Earth Syst. Sci. Data.* 12 (1), 753–769. doi:10.5194/essd-12-753-2020

Perry, S. J., McGregor, S., Gupta, A. S., and England, M. H. (2017). Future changes to El niño–southern oscillation temperature and precipitation teleconnections. *Geophys. Res. Lett.* 44 (20), 10,608–10,616. doi:10.1002/2017GL074509

Prajapati, V. K., Khanna, M., Singh, M., Kaur, R., Sahoo, R. N., and Singh, D. K. (2021). Evaluation of time scale of meteorological, hydrological and agricultural drought indices. *Nat. Hazards* 109 (1), 89–109. doi:10.1007/s11069-021-04827-1

Qian, D. L., and Guan, Z. Y. (2018). Different features of super and regular El Niño events and their impacts on the variation of the West Pacific Subtropical High. *Acta. Meteorol. Sin.* 76 (3), 394–407.

Richman, M. B. (1986). Rotation of principal components. *J. Climatol.* 6 (3), 293–335. doi:10.1002/joc.3370060305

Rutledge, D. N. (2018). Comparison of principal components analysis, independent components analysis and common components analysis. *J. Anal. Test.* 2 (3), 235–248. doi:10.1007/s41664-018-0065-5

Şen, Z., Şişman, E., and Dabanli, I. (2020). Wet and dry spell feature charts for practical uses. *Nat. Hazards.* 104 (3), 1975–1986. doi:10.1007/s11069-020-04257-5

Shen, X. L., Zhu, C. W., and Li, M. (2012). Possible causes of persistent drought event in North China during the cold season of 2010. *Chin. J. Atmos. Sci.* 06, 1123–1134.

Singh, J., Ashfaq, M., Skinner, C. B., Anderson, W. B., Mishra, V., and Singh, D. (2022). Enhanced risk of concurrent regional droughts with increased ENSO variability and warming. *Nat. Clim. Change.* 12 (2), 163–170. doi:10.1038/s41558-021-01276-3

Su, B., Huang, J., Fischer, T., Wang, Y., Kundzewicz, Z. W., Zhai, J., et al. (2018). Drought losses in China might double between the 1.5 C and 2.0 C warming. *Proc. Natl. Acad. Sci.* 115 (42), 10600–10605. doi:10.1073/pnas.1802129115

Su, Y., Lu, C. Y., Huang, Y. F., Su, Y. L., Wang, Z. L., and Lei, Y. F. (2022). Quantitative analysis of spatio-temporal evolution characteristics of seasonal average maximum temperature and its influence by atmospheric circulation in China from 1950 to 2019. *Environ. Sci.* doi:10.13227/j.hjkx.202205258

Sun, B. F., Zhao, H., and Wang, X. K. (2015). Spatiotemporal characteristics of drought in Northeast China based on SPEI. *Ecol. Environ.* 24 (1), 22–28.

Thornthwaite, C. W. (1948). An approach toward a rational classification of climate. *Geogr. Rev.* 66, 77–94. doi:10.1097/00010694-194807000-00007

Trenberth, K. E., Dai, A., Van Der Schrier, G., Jones, P. D., Barichivich, J., Briffa, K. R., et al. (2014). Global warming and changes in drought. *Nat. Clim. Change* 4 (1), 17–22. doi:10.1038/NCLIMATE2067

Vicente Serrano, S. M. (2005). El Niño and La Niña influence on droughts at different timescales in the iberian peninsula. *Water Resour. Res.* 41 (12). doi:10.1029/2004WR003908

Vicente-Serrano, S. M., Beguería, S., and López-Moreno, J. I. (2010). A multiscalar drought index sensitive to global warming: The standardized precipitation evapotranspiration index. *J. Clim.* 23 (7), 1696–1718.

Wang, F., Ding, J. L., and Wei, Y. (2017). Analysis of drought characteristics over countries and regions of "The Belt and Road" in recent one hundred years. *Geo-inf Sci.* 19 (11), 1442–1455. doi:10.3724/SP.J.1047.2017.01442

Wang, J. R., Sun, C. G., Zheng, Z. J., and Li, X. M. (2021). Drought characteristics of the Loess Plateau in the past 60 years and itsrelationship with changes in atmospheric circulation. *Acta. Ecol. Sin.* 41 (13), 5340–5351.

Wang, T., Li, S. S., Yan, J. P., and He, J. P. (2022b). Spatio-temporal variation of summer precipitation in China based on ENSO development process. *J. Nat. Resour.* 37 (03), 803–815. doi:10.31497/zrzyxb.20220316

Wu, P., Ding, Y. H., and Liu, Y. J. (2017). A new study of El Nifino impacts on summertime water vapor transport and rainfall in China. *Acta Meteorol. Sin.* 03, 371–383.

Xu, Y., Zhang, X., Hao, Z., Singh, V. P., and Hao, F. (2021). Characterization of agricultural drought propagation over China based on bivariate probabilistic quantification. *J. Hydro.* 598, 126194. doi:10.1016/j.jhydrol.2021.126194

Xue, F., and Zhao, J. J. (2017). Intraseasonal variation of the East Asian summer monsoon in La Niña years. *Atmos. Ocean. Sci. Lett.* 10 (2), 156–161. doi:10.1080/16742834.2016.1254008

Yan, Z. X. (2022). "A study of ENSO precipitation anomaly diversity and its change in the context of global warming,". [dissertation's thesis] (Nanjing: Nanjing University of Information Science & Technology).

Yang, T. Z., Zhang, H. B., Li, Y. B., Lv, F. G., Wang, Y. W., and Yao, C. C. (2022). *Investigating dynamics characteristics and spatial distribution of monthly precipitation time series in the Weihe River Basin using sample entropy*. Xi'an: Yellow River. 1-6[2023-04-14]. http://kns.cnki.net/kcms/detail/41.1128.TV.20230303.1056.002.html.

Yeh, S. W., Cai, W., Min, S. K., McPhaden, M. J., Dommenget, D., Dewitte, B., et al. (2018). ENSO atmospheric teleconnections and their response to greenhouse gas forcing. *Rev. Geophys.* 56 (1), 185–206. doi:10.1002/2017RG000568

Yue, S. Y., Li, H. E., and Zhao, L. (2021). Impact of climate and land use changes on water scarcity in the Wei River basin. *Res. Soil Water Conserv* 28 (5), 95–101. doi:10.13869/j.cnki.rswc

Zhang, X. R., Cai, Y. R., Zhao, J., and Gao, Z. L. (2010). Caused harm of soil erosion in the Loess Plateau and its comprehensive control measures. *J. Anhui Agric. Sci.* 38 (28), 15776–15781. doi:10.13989/j.cnki.0517-6611.2010.28.074

Zhang, C. M., Wu, S. S., and Huang, C. T. (2021). Characteristics of atmospheric circulationforspring precipitation anomalies in Jiangxi Province and its response to ENSO Events. *Torr Rain Disas* (04), 410–418.

Zhang, D. Q., Yuan, Y., and Han, R. Q. (2023). Characteristics and possible causes of the climate anomalies over China in summer 2022. *Meteor. Mon.* 49 (1), 110–121.

Zhang, L., He, Z. H., Yang, M. K., You, M., and Pi, G. N. (2022a). Characteristics of meteorological drought-hydrological drought propagation process and its influencing factors-taking guizhou qianzhong water conservancy project area as an example. *J. Soil Water Conserv.* (01), 142–152. doi:10.13870/j.cnki.stbcxb.2022.01.020

Zhang, L., Wu, P., Zhou, T., and Xiao, C. (2018b). ENSO transition from La Niña to El Niño drives prolonged spring–summer drought over North China. *J. Clim.* 31 (9), 3509–3523. doi:10.1175/JCLI-D-17-0440.1

Zhang, Q., Han, L. Y., Lin, J. J., and Cheng, Q. Y. (2018a). North–South differences in Chinese agricultural losses due to climate–change–influenced droughts. *Theor. Appl. Clim.* 131 (1), 719–732. doi:10.1007/s00704-016-2000-x

Zhang, Q. Y., Tao, S. Y., and Peng, J. B. (2008). The studies of meteorological disasters over China. *Chin. J. Atmos. Sci.* (04), 815.

Zhang, T., Su, X., Zhang, G., Wu, H., Wang, G., and Chu, J. (2022b). Evaluation of the impacts of human activities on propagation from meteorological drought to hydrological drought in the Weihe River Basin, China. *Sci. Total Environ.* 819, 153030. doi:10.1016/j.scitotenv.2022.153030

Zhang, W., Jin, F. F., and Turner, A. (2014). Increasing autumn drought over southern China associated with ENSO regime shift. *Geophys. Res. Lett.* 41 (11), 4020–4026. doi:10.1002/2014GL060130

Zhao, P. P., Lv, H. S., and Wang, C. Y. (2018). Impact of ENSO event on meteorological drought and hydrological drought in Weihe River Basin. *Water Resour. Power* (08), 9–13.

Zhao, S. Y., Chen, L. J., and Cui, T. (2017). Effects of ENS0 phase-switching on rainy-season precipitation in North China. *Chin. J. Atmos. Sci.* 41 (4), 857–868. doi:10.3878/j.issn.1006-9895.1701.16226

Zheng, F., Liu, J. P., Fang, X. H., Song, M. R., Yang, C. Y., Yuan, Y., et al. (2022). The predictability of ocean environments that contributed to the 2020/21 extreme cold events in China: 2020/21 La Niña and 2020 arctic sea ice loss. *Adv. Atmos. Sci.* 39 (4), 658–672. doi:10.1007/s00376-021-1130-y

Zheng, F., Yuan, Y., Ding, Y., Li, K., Fang, X., Zhao, Y., et al. (2021). The 2020/21 extremely cold winter in China influenced by the synergistic effect of La Niña and warm Arctic. *Adv. Atmos. Sci.* 39 (4), 546–552. doi:10.1007/s00376-021-1033-y

Zhou, L., Wang, S., Chi, Y., and Wang, J. (2018). Drought impacts on vegetation indices and productivity of terrestrial ecosystems in southwestern China during 2001–2012. *Chin. Geogr. Sci.* 28 (5), 784–796. doi:10.1007/s11769-018-0967-1

Zhou, T., Wu, B., and Dong, L. (2014). Advances in research of ENSO changes and the associated impacts on Asian-Pacific climate. *Asia-Pac. J. Atmos. Sci.* 50 (4), 405–422. doi:10.1007/s13143-014-0043-4

Zhou, X., Huang, G., Fan, Y., Wang, X., and Li, Y. (2022). A mixed-level factorial inference approach for ensemble long-term hydrological projections over the Jing River Basin. *J. Hydrometeorol.* 23 (11), 1807–1830. doi:10.1175/jhm-d-21-0158.1